Photoionization processes of the beryllium atom

Ju-Tang Hsiao,[1] Lin-Ru Wang,[1] Hsiao-Ling Sun,[1,2] Sheng-Fang Lin,[1,2] Cheng-Liang Lu,[1,2] and Keh-Ning Huang[1,2]
[1]*Institute of Atomic and Molecular Sciences, Academia Sinica, P.O. Box 23-166, Taipei, Taiwan 106, Republic of China*
[2]*Department of Physics, National Taiwan University, Taipei, Taiwan 106, Republic of China*
(Received 23 April 2008; revised manuscript received 27 May 2008; published 17 July 2008)

The cross section σ, angular-distribution parameter β, and spin-polarization parameters $\{\xi, \eta, \zeta\}$ of photoelectrons for neutral beryllium are calculated in the multiconfiguration relativistic random-phase approximation theory. Precise energies and widths of all five Rydberg series of doubly excited states $(2pns)^1P_1^o$, $(2pns)^3P_1^o$, $(2pnd)^1P_1^o$, $(2pnd)^3P_1^o$, and $(2pnd)^3D_1^o$ are given. Experimental studies of the angular distribution and spin polarization of photoelectrons are suggested to obtain information on energies and widths of states, which cannot be obtained from total cross-section measurements.

DOI: 10.1103/PhysRevA.78.013411 PACS number(s): 32.80.Fb, 31.15.ap, 31.15.aj

I. INTRODUCTION

Photoionization processes are of fundamental importance as well as crucial to astrophysical modeling and other applications. The study of photoionization processes provides a simple way to analyze electron correlation and relativistic effects in atoms and ions. Further theoretical studies of photoionization of atoms and ions are of interest because recent improvements in experimental techniques have greatly enhanced the ability to make precise measurements.

In recent years, a great deal of attention has been paid to multielectron excitations in open-shell atoms. Double-electron resonances in the photoionization spectrum of alkaline-earth-metal atoms are the most prominent feature for photon energies just above the first ionization threshold and have been the focus of many theoretical and experimental studies. Among theoretical methods employed for the study of double excitations, there are many-body perturbation theory [1–4], the close-coupling method [5–9], the configuration-interaction formalism [10–14], the model-potential calculation [15], the complex-basis expansion method [16], the generalized hyperspherical coordinate method [17,18], the random-phase approximation [19,20], the relativistic random-phase approximation [21,22], the multiconfiguration relativistic Tamm-Dancoff approximation [23], multiconfiguration Hartree-Fock theory [24], the *R*-matrix method [25], and the multiconfiguration relativistic random-phase approximation (MCRRPA) [26–29].

Because beryllium is the simplest two-valence atom, it should be an atom suitable for comprehensive studies of correlation and relativistic effects in photoionization processes. With low-lying doubly excited states in the energy range between the first and second ionization thresholds of the neutral beryllium atom, double-excitation autoionization resonances are the most prominent feature in its photoionization spectrum. These double-excitation resonances in the photoionization spectrum reveal correlation and relativistic effects and therefore provide a stringent testing ground for the accuracy of theoretical models.

The photoabsorption spectrum from the ground-state beryllium atom was measured by Mehlman-Balloffet and Esteva [30], in which a few double-excitation resonances $(2pns)^1P_1^o$ and $(2pnd)^1P_1^o$ with $n \geqslant 3$ were identified, and the emission spectrum was later reported by Esteva *et al.* [31]. The most recent experimental work was given by Wehlitz *et al.* [32] employing monochromatized synchrotron radiation.

Positions and widths of a few double-excitation resonances in the photoionization spectrum of the beryllium atom were first calculated by Moores [5] by using the close-coupling method. The photoionization cross section above the first ionization threshold of the ground-state beryllium atom was calculated by Altick [10] by using the configuration-interaction method. Subsequently, the main features of the photoionization cross section of the neutral beryllium atom have been studied by numerous researches, among them, Laughlin and Victor [15] by using a model-potential approach, Dubau and Wells [7] by using the quantum-defect theory, Amusia *et al.* [20] by using the random-phase approximation, Johnson and Lin [21] by using the RRPA, Lee and Johnson [33] by using the multichannel quantum-defect theory, Lin [34] by using hyperspherical coordinates, Radojevic and Johnson [23] by using the multiconfiguration relativistic Tamm-Dancoff approximation, Moccia and Spizzo [14] by using variational wave functions, Chi *et al.* [29] by using the MCRRPA, Chang and Zhu [35] by using the configuration-interaction method, Zhou and Lin [36] by using the hyperspherical close-coupling method, and Kim *et al.* [37] by using the *R*-matrix method.

In the photon-energy region between $(1s^22s)^2S_{1/2}$ and $(1s^22p)^2P_{1/2}$ ionization thresholds of the beryllium atom, double-excitation resonances in the photoionization spectrum may be classified into five Rydberg series: $(2pns)^1P_1^o$, $(2pns)^3P_1^o$, $(2pnd)^1P_1^o$, $(2pnd)^3P_1^o$, and $(2pnd)^3D_1^o$. Most of the earlier nonrelativistic studies focused only on resonances $(2pns)^1P_1^o$ and $(2pnd)^1P_1^o$. Because of the incorporation of relativity in the MCRRPA, the double-excitation resonances in the photoionization spectrum belonging to all five Rydberg series of the beryllium atom are built in from the outset [29]. Applications of the MCRRPA to photoexcitation [27,38,40] and photoionization [29,41–43] of atoms or ions with two valence electrons have been very successful.

The main concerns of most photoionization researches are with the cross sections. Nevertheless, a complete macroscopic analysis of photoionization processes requires also knowledge of the angular distribution and spin polarization

of photoelectrons. In the nonrelativistic limit, these extra parameters are all constants; however, recent works have shown relativistic effects to be important in the photoionization of small atoms, such as Be [29], Ne [44], and Mg [41,45,46]. Therefore, it is worthwhile to investigate the interplay between correlation and relativistic effects on the photoionization of atoms or ions with a very low nuclear charge. In this work for the photoionization of neural beryllium by using the MCRRPA, the cross section, angular distribution, and spin polarization of photoelectrons are studied in detail, accounting for all relativistic excitation channels. Additionally, we shall study in detail the positions and widths of all these double-excitation resonances of the beryllium atom. A preliminary result of this work has been published [47]. In Sec. II we review our method briefly. Results are presented in Sec. III, and the conclusion is made in Sec. IV.

II. MCRRPA THEORY

The MCRRPA theory [26] for an N-electron atom or ion is based on the relativistic Hamiltonian

$$H(t) = H_0 + V(t), \tag{1}$$

where

$$H_0 = \sum_{i=1}^{N} h_i + \sum_{i<j}^{N} \frac{e^2}{r_{ij}}, \tag{2}$$

$$V(t) = v_+ e^{-it\omega} + v_- e^{i\omega t}, \tag{3}$$

where h_i is the single-electron Dirac Hamiltonian, $V(t)$ is the external potential that induces transitions between atomic states, and the perturbing fields $v_\pm$ are sums of electric and magnetic multipole potentials [26,48].

We describe the N-electron system as a superposition of configuration wave functions with time-dependent weights. Applying the variational principle, we derive time-dependent multiconfiguration Dirac-Fock equations describing the response of the atom to the external field. Terms independent of the external field lead to the usual stationary multiconfiguration Dirac-Fock (MCDF) equations; terms proportional to the external field lead to equations describing the linear response of the atomic state to the external field. We refer to these linear-response equations as the multiconfiguration relativistic random-phase approximation equations. If we start from a single-configuration reference state, the MCRRPA equations reduce to the RRPA equations.

In our application of the MCRRPA to the photoionization of the beryllium atom in its ground state, the multiconfiguration reference state is described by the linear combination of three configurations with two valence electrons coupled to zero angular momentum and even parity:

$$\Psi = C_1(1s_{1/2}^2 2s_{1/2}^2)_0 + C_2(1s_{1/2}^2 2p_{1/2}^2)_0 + C_3(1s_{1/2}^2 2p_{3/2}^2)_0, \tag{4}$$

where C_1, C_2, and C_3 are configuration-weight coefficients.

We consider seven excitation channels from the valence electrons in the electric-dipole approximation for photon energies between $(1s^2 2s)S_{1/2}^2$ and $(1s^2 2p)P_{1/2}^2$ ionization thresholds. The actual MCRRPA calculations are done in the jj coupling, in which couplings between fully relativistic channels are treated. On the other hand, physical interpretations are more readily given in the LS coupling for a lighter element such as Be. Nevertheless, jj coupling channels and LS-coupling channels are related by simple transformation formulas. Classified in the LS coupling notation, the seven excitation channels are the following:

(i) Photoionization channels:
(a) $(2s^2)1\,^1S_0 \rightarrow (2s\epsilon p)\,^1P_1^o$,
(b) $(2s^2)\,^1S_0 \rightarrow (2s\epsilon p)\,^3P_1^o$.
(ii) Photoexcitation channels:
(c) $(2s^2)\,^1S_0 \rightarrow (2pns)\,^1P_1^o$, $n \geq 3$,
(d) $(2s^2)\,^1S_0 \rightarrow (2pns)\,^3P_1^o$,
(e) $(2s^2)\,^1S_0 \rightarrow (2pnd)\,^1P_1^o$,
(f) $(2s^2)\,^1S_0 \rightarrow (2pnd)\,^3P_1^o$,
(g) $(2s^2)\,^1S_0 \rightarrow (2pnd)\,^3D_1^o$.

The couplings between the *photoionization* and *photoexcitation channels* generate five autoionization resonance series in the photoionization spectrum.

Photoionization of unpolarized atoms or ions in the dipole approximation can be completely described by a set of five dynamical parameters [49–51]: namely, the total cross section σ, the angular-distribution parameter β, and spin-polarization parameters ξ, η, and ζ. At the photon energy $\hbar\omega$, these dynamical parameters for the photoionization of beryllium can be expressed in terms of photoionization amplitudes $|D_S|$ and $|D_T|$, and their relative phase $\phi \equiv \phi_S - \phi_T$, where the subscripts S and T denote, respectively, the singlet and triplet channels:

$$\sigma = \frac{8\pi^4}{\omega c}(|D_S|^2 + |D_T|^2), \tag{5}$$

$$\beta = \frac{2|D_S|^2 - |D_T|^2}{(|D_S|^2 + |D_T|^2)}, \tag{6}$$

$$\xi = \frac{3}{\sqrt{2}} \frac{|D_S||D_T|\cos\phi}{(|D_S|^2 + |D_T|^2)}, \tag{7}$$

$$\eta = \frac{3}{\sqrt{2}} \frac{|D_S||D_T|\sin\phi}{(|D_S|^2 + |D_T|^2)}, \tag{8}$$

$$\zeta = \frac{3|D_T|^2}{2(|D_S|^2 + |D_T|^2)} = 1 - \frac{1}{2}\beta. \tag{9}$$

Here the LS-coupling amplitudes D_S and D_T are related to the jj-coupling amplitudes $D_{p_{1/2}}$ and $D_{p_{3/2}}$ as

$$D_S = \frac{1}{\sqrt{3}}(D_{p_{1/2}} + \sqrt{2}D_{p_{3/2}}), \tag{10}$$

$$D_T = \frac{1}{\sqrt{3}}(-\sqrt{2}D_{p_{1/2}} + D_{p_{3/2}}). \tag{11}$$

We note particularly that for photoionization of an unpolarized beryllium atom only three of the five parameters

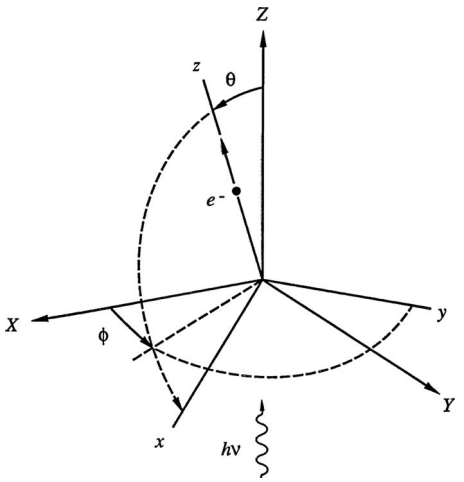

FIG. 1. Geometrical relationships used in the angular-distribution and spin-polarization formulas. The photon is incident along the Z axis, and the ejected photoelectron is along the z axis.

$\{\sigma, \beta, \xi, \eta, \zeta\}$ are independent, which may be expressed in terms of three independent quantities $\{|D_S|, |D_T|, \phi\}$.

We define a fixed coordinate system (XYZ) at the target such that the Z axis is in the direction of the photon flux. We also define a rotated coordinate system (xyz) obtained from the fixed coordinate system (XYZ) by rotations with Euler angles $(\varphi, \theta, 0)$. The rotated coordinate system (xyz) is chosen such that the z axis, making an angle θ with the Z axis, is the direction of the outgoing photoelectron and the y axis is perpendicular to both the Z and z axes. The spin polarization of the photoelectron is defined with respect to the rotated coordinate system (xyz). The relative orientation of these two coordinate systems is shown in Fig. 1. The angular distribution and spin polarization of photoelectrons for circularly polarized photons are given, for example, by [49]

$$\frac{d\sigma}{d\Omega} = \frac{\sigma}{4\pi}\left(1 - \frac{1}{2}\beta P_2(\cos\theta)\right), \tag{12}$$

$$P_x(\theta,\varphi) = \pm \frac{\xi \sin\theta}{\left[1 - \frac{1}{2}\beta P_2(\cos\theta)\right]}, \tag{13}$$

$$P_y(\theta,\varphi) = \frac{\eta \sin\theta\cos\theta}{\left[1 - \frac{1}{2}\beta P_2(\cos\theta)\right]}, \tag{14}$$

$$P_z(\theta,\varphi) = \pm \frac{\zeta \cos\theta}{\left[1 - \frac{1}{2}\beta P_2(\cos\theta)\right]}, \tag{15}$$

where the $\pm$ signs are for photon with positive or negative helicity.

TABLE I. Configuration weights of the beryllium atom in its ground state $j=0$ even.

Configuration	Weight	Percentage
$1s^2_{1/2}2s^2_{1/2}$	0.950	90.3
$1s^2_{1/2}2p^2_{1/2}$	0.180	3.2
$1s^2_{1/2}2p^2_{3/2}$	0.255	6.5

III. RESULTS AND DISCUSSIONS

The MCRRPA theory has been applied for the photoionization of beryllium to calculate transition amplitudes $D_{p_{1/2}}$ and $D_{p_{3/2}}$ for the jj-coupling channels $(2s^2_{1/2})_0 \rightarrow (2s_{1/2}\epsilon p_{1/2})^o_1$ and $(2s^2_{1/2})_0 \rightarrow (2s_{1/2}\epsilon p_{3/2})^o_1$, respectively. In Table I, we present the configuration-weight coefficients and their percentage from MCDF theory. We note that while the dominant configuration is the $(1s^2_{1/2}2s^2_{1/2})_0$ configuration, the others also have significant contributions and thus play important roles in photoionization processes. The use of a multiconfiguration wave function as the reference state improved the agreement between theoretical and experimental results.

The energy spectrum of the beryllium atom is given in Fig. 2, which consists of bound and continuum states. The five doubly excited Rydberg series manifest themselves as pseudobound states in the figure. Calculated cross sections σ for photon energies from 0.360 a.u. to 0.483 a.u., are presented in Fig. 3 as a demonstration. The dotted curve is for the RRPA results, in which *photoionization channels* (a) and (b) are included while the ground state of Be is approximated only by a single-configuration $(1s^2 2s^2)^1S_0$; therefore, double-excitation resonances are not present in the RRPA photoionization spectrum. The dashed curve is for the MCRRPA(0) calculation with the same *photoionization channels* (a) and (b), in which the ground state of Be is, however, more

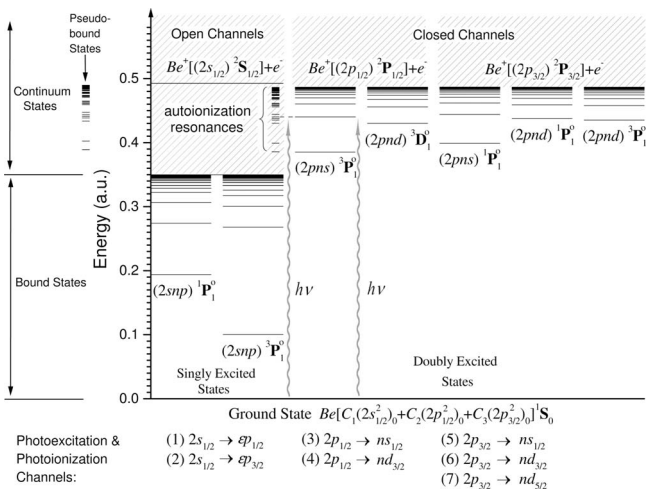

FIG. 2. The energy spectrum of beryllium. Seven Rydberg series $2snp(^1P^o_1, ^3P^o_1)$, $2pns(^1P^o_1, ^3P^o_1)$, $2pnd(^1P^o_1, ^3P^o_1)$, and $2pnd(^3D^o_1)$ are shown.

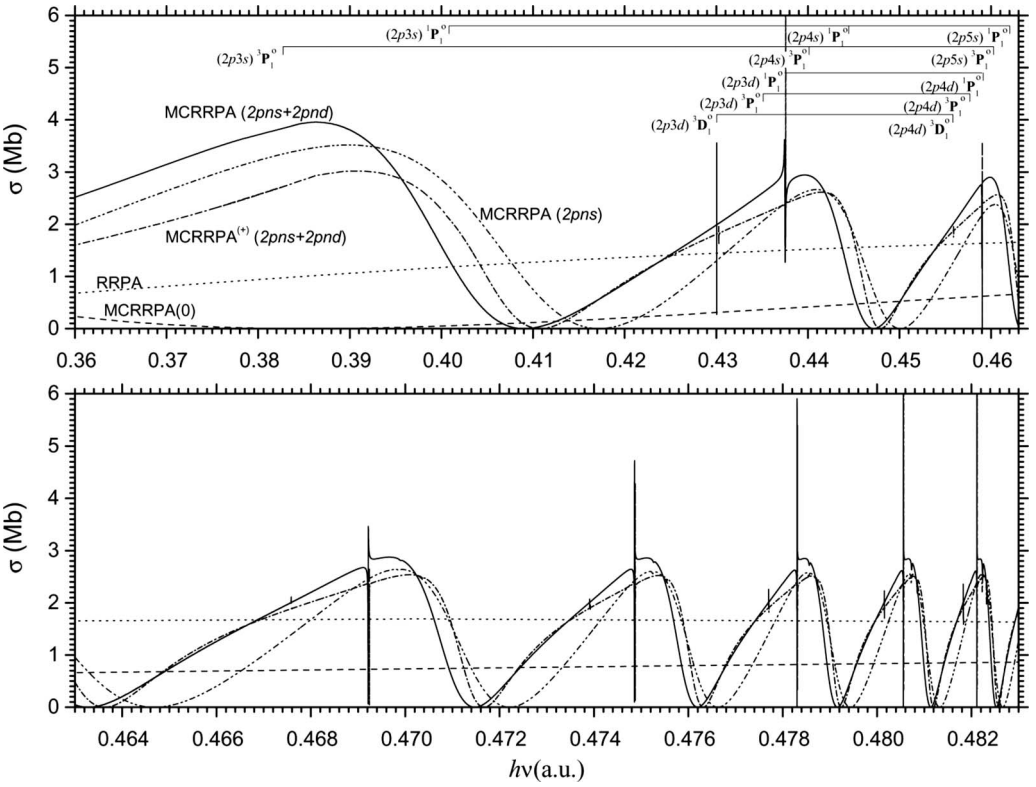

FIG. 3. Cross sections σ as a function of the photon energy in a.u. The dotted and dashed curves are for the RRPA and MCRRPA(0) calculations, respectively. The solid curve represents the MCRRPA($2pns+2pnd$) calculation which includes all five Rydberg series, while the dash-dotted curve represents the MCRRPA$^{(+)}$($2pns+2pnd$) calculation which includes only positive-frequency Feynman diagrams dealing with the final-state RPA-type correlations. The dash-dot-dotted curve represents the MCRRPA($2pns$) calculation which includes only the ($2pns$) resonances.

accurately described by a mixture of two configurations $(1s^22s^2)^1S_0$ and $(1s^22p^2)^1S_0$ through the weight coefficients even without relativistic effects. However, without treating couplings to *photoexcitation channels*, this MCRRPA(0) calculation reveals no resonance structure, but only a characteristic Cooper minimum as in an independent-particle model. Therefore, the effects of excited configurations in the ground-state wave function pull the Cooper minimum outside the $(1s^22s)^2S_{1/2}$ threshold.

By including two *photoexcitation channels* (c) and (d) associated with resonances $(2pns)^1P_1^o$ and $(2pns)3^3P_1^o$ in addition to photoionization channels (a) and (b), the four-channel MCRRPA($2pns$) results are also shown in Fig. 3. Consequently, the MCRRPA(0) curve with a characteristic Cooper minimum is then replaced by the dash-dotted MCRRPA ($2pns$) curve, which shows broad resonance structures primarily due to resonances $(2pns)^1P_1^o$, with the effects of resonances $(2pns)^3P_1^o$ completely masked by those of resonances $(2pns)^1P_1^o$. These $(2pns)^3P_1^o$ resonances are due to relativistic effects, without which they are completely forbidden; it is rather remarkable that they show up for a low-Z element like beryllium.

The solid curve in Fig. 3 represents the seven-channel MCRRPA($2pns+2pnd$) calculation which includes all five Rydberg series of resonances involving both ($2pns$) and ($2pnd$) subshells, and the vertical tic marks show the positions of corresponding resonances derived from the phase-shift variations. Because the photoionization continuum $(2s\epsilon p)^1P_1^o$ and the double-excitation series $(2pns)^1P_1^o$ and $(2pnd)^1P_1^o$ all arise from the $n=2$ atomic complex and with the same total spin and orbital angular momenta, the couplings between them are strong such that the characteristics of the cross sections are completely dominated by double-excitation resonances $(2pns)^1P_1^o$ and $(2pnd)^1P_1^o$. Experimentally or in a nonrelativistic calculation, the cross section should be similar to the MCRRPA ($2pns+2pnd$) results but without the extremely sharp resonance structures of triplet resonances $(2pnd)^3D_1^o$. The dash-dotted curve in Fig. 3 represents the MCRRPA$^{(+)}$($2pns+2pnd$) calculation which includes only positive-frequency Feynman diagrams dealing with the final-state RPA-type correlations. The difference between curves MCRRPA($2pns+2pnd$) and MCRRPA$^{(+)}$($2pns+2pnd$) shows the effects of initial-state RPA-type correlations, which shift $(2pns)^1P_1^o$ resonance energies slightly to the left. Photoionization cross sections σ and corresponding phase shifts δ of the first five resonances are shown in Fig. 4 as a demonstration, where the phase shift δ goes through π in the neighborhood of each resonance.

The precise positions and widths of double-excitation resonances belonging to five Rydberg series for the MCRRPA($2pns+2pnd$) calculation are inferred from the phase shifts. In Tables II and III, we present the resonance energies E_r of allowed doubly excited states, $(2pns)^1P_1^o$ and $(2pnd)^1P_1^o$, respectively. Tables IV and V list the correspond-

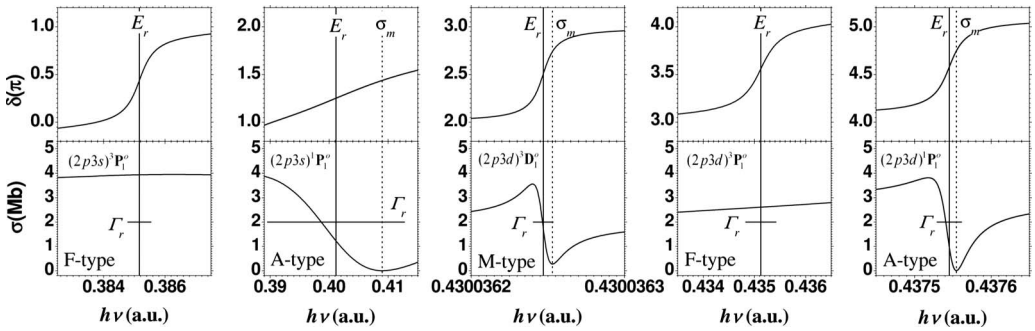

FIG. 4. Photoionization cross sections σ and corresponding phase shifts δ for the first five resonances. Here σ_m indicates the cross-section minimum, E_r the resonance energy, and Γ_r the width of the resonance.

ing resonance widths Γ_r of $(2pns)^1P_1^o$ and $(2pnd)^1P_1^o$. Resonance energies E_r and widths Γ_r of forbidden doubly excited states $(2pns)^3P_1^o$, $(2pnd)^3P_1^o$, and $(2pnd)^3D_1^o$ are shown in Table VI. It shows a fair agreement of our MCRRPA $(2pns+2pnd)$ calculation for energy positions and resonance widths with those of other theories and with experiment. Because the orbital symmetries of the photoionization channels $(2s\epsilon p)^3P_1^o$ and $(2s\epsilon p)^1P_1^o$ are of P type, the coupling of resonances $(2pnd)^3D_1^o$ with these photoionization channels are weaker such that their widths are much narrower. There are, however, large discrepancies between theoretical results for resonance widths. Our calculation, which deals with all five Rydberg series, includes more correlation and relativistic effects than all of the other calculations and, moreover, treats the initial and final states in a balanced fashion; therefore, it should in principle provide the most precise lifetimes theoretically. Nevertheless, further new schemes of experiments are needed to resolve these discrepancies.

The comparison of our photoionization cross section with those of selected other theories and with experiment is presented in Fig. 5. The profiles and positions of autoionization resonances from the MCRRPA agree very well with experiment.

The angular-distribution and spin-polarization parameters $\{\beta,\xi,\eta,\zeta\}$, which have pronounced variations in the vicinity of each double-excitation resonance, display primarily three classes of characteristic behaviors, *A* Type for *allowed* resonances $(2pns)^1P_1^o$ and $(2pnd)^1P_1^o$, *F* Type for *forbidden* resonances $(2pns)^3P_1^o$ and $(2pnd)^3P_1^o$, and *M* Type for *forbidden* resonances $(2pnd)^3D_1^o$, which resemble a *mixture* of *A* type and *F* type. The angular-distribution parameter β, spin-polarization parameters ξ and η, singlet transition amplitude $|D_S|^2$, triplet transition amplitude $|D_T|^2$, and their relative phase ϕ for the first five resonances $(2p3s)^3P_1^o$, $(2p3s)^1P_1^o$, $(2p3d)^3D_1^o$, $(2p3d)^3P_1^o$, and $(2p3d)^1P_1^o$ are given in Fig. 6 as a demonstration. These parameters deviate from their nonrelativistic limits due to relativistic effects which permit couplings with forbidden channels. In the nonrelativistic limit, the final state should be of the $^1P_1^o$ type and $D_T=0$ such that $\beta=2$ and $\xi=\eta=\zeta=0$. Relativistic effects cause deviations from these limits.

A. *A*-type resonances

Characteristics of photoionization parameters for *allowed* resonances $(2pns)^3P_1^o$ and $(2pnd)^1P_1^o$ are similar and will be

TABLE II. Resonance energies E_r (in a.u.) of doubly excited states $(2pns)^1P_1^o$ of Be. Reference numbers are shown in brackets.

	Theories								Experiments		
States	MCRRPA	[5]	[10]	[15]	[34]	[39]	[35]	[37]	[30]	[31]	[32]
$(2p3s)^1P_1^o$	0.401143	0.40387	0.39579	0.39321	0.39000	0.40112	0.40167	0.40094	0.3935	0.4018	0.4002
$(2p4s)^1P_1^o$	0.444445	0.44577	0.44356	0.44283	0.43970	0.44474	0.44503	0.44436	0.4398	0.4445	0.4451
$(2p5s)^1P_1^o$	0.462043	0.46304	0.46304	0.46157		0.46197	0.46230	0.46149	0.4606	0.4620	0.4620
$(2p6s)^1P_1^o$	0.470814			0.47076		0.47039	0.47112	0.47006	0.4697	0.4708	0.4708
$(2p7s)^1P_1^o$	0.475803					0.47524		0.47494	0.4749	0.4757	0.4775
$(2p8s)^1P_1^o$	0.478907							0.47799	0.4781	0.4788	0.4785
$(2p9s)^1P_1^o$	0.480968							0.48003		0.4808	0.4806
$(2p10s)^1P_1^o$	0.482406							0.48145		0.4822	0.4823
$(2p11s)^1P_1^o$	0.483449							0.48247		0.4833	0.4830
$(2p12s)^1P_1^o$	0.484229							0.48324		0.4840	0.4843
$(2p13s)^1P_1^o$	0.484829							0.48384			
$(2p14s)^1P_1^o$	0.485233							0.48430			
$(2p15s)^1P_1^o$	0.485675							0.48468			

TABLE III. Resonance energies E_r(in a.u.) of doubly excited states $(2pnd)^1P_1^o$ of Be. Reference numbers are shown in brackets.

	Theories								Experiments		
States	MCRRPA	[5]	[10]	[15]	[34]	[39]	[35]	[37]	[30]	[31]	[32]
$(2p3d)^1P_1^o$	0.437546	0.43842	0.43584	0.43474	0.43245	0.43511	0.43584	0.43478	0.4359	0.4357	0.4351
$(2p4d)^1P_1^o$	0.458992	0.46010	0.45826	0.45789	0.45475	0.45745	0.45826	0.45706	0.4581	0.4595	0.4579
$(2p5d)^1P_1^o$	0.469214					0.46800	0.46892	0.46771	0.4688	0.4700	0.4683
$(2p6d)^1P_1^o$	0.474858					0.47381		0.47356	0.4748	0.4760	
$(2p7d)^1P_1^o$	0.478303							0.47711			
$(2p8d)^1P_1^o$	0.480559							0.47942			
$(2p9d)^1P_1^o$	0.482116							0.48102			
$(2p10d)^1P_1^o$	0.483236							0.48215			
$(2p11d)^1P_1^o$	0.484068							0.48300			
$(2p12d)^1P_1^o$	0.484704							0.48365			
$(2p13d)^1P_1^o$	0.485199							0.48415			
$(2p14d)^1P_1^o$	0.485594							0.48455			
$(2p15d)^1P_1^o$	0.485912							0.48487			

classified as of A type. Specifically, results of angular-distribution parameters β, spin-polarization parameters ξ and η, singlet transition amplitude $|D_S|^2$, triplet transition amplitude $|D_T|^2$, and their relative phase ϕ for resonance $(2p3s)^1P_1^o$ and $(2p3d)^1P_1^o$ are given in Fig. 6. The behavior of angular distribution parameter β is easily understood by considering Eq. (6) and can be summarized as follows.

(i) Around the A-type resonance, we observe marked departures of β from its background value 2, and β reaches its minimum -1 at the resonance minimum σ_m.

(ii) Slightly away from the singlet resonances $(2pns)^1P_1^o$ and $(2pnd)^1P_1^o$, $|D_S| \gg |D_T|$ such that $\beta=2$.

(iii) At the resonance minimum, the singlet amplitude $|D_S|$ goes through zero such that Eq. (6) yields $\beta=-1$, no matter how small $|D_T|$ is, as long as it does not vanish at that energy.

The interesting *detuning* of spin-polarization parameters ξ and η around the resonance minimum may be understood with the following reasons.

(i) The singlet amplitude $|D_S|$ goes through zero at a resonance minimum and varies linearly as a function of the energy departure from the resonance minimum.

(ii) The triplet amplitude $|D_T|$ stays fairly constant in this small energy range.

(iii) The relative phase ϕ goes through π rapidly in the immediate neighborhood around the resonance minimum but seems to be fairly constant away from the resonance.

(iv) $\xi \simeq \frac{3}{\sqrt{2}}|\frac{D_S}{D_T}|\cos\phi$ and $\eta \simeq \frac{3}{\sqrt{2}}|\frac{D_S}{D_T}|\sin\phi$ around the resonance minimum, and $\xi \simeq \frac{3}{\sqrt{2}}|D_T D_S|\cos\phi$ and $\eta \simeq \frac{3}{\sqrt{2}}|\frac{D_T}{D_S}|\sin\phi$ away from the resonance.

TABLE IV. Resonance widths Γ_r (in a.u.) of doubly excited states $(2pns)^1P_1^o$ of Be. Numbers in brackets parentheses indicate powers of 10. Reference numbers are shown in brackets.

	Theories						Experiment
States	MCRRPA	[5]	[17]	[39]	[35]	[37]	[32]
$(2p3s)^1P_1^o$	2.3205(−2)	1.34(−2)	1.94770(−2)	2.22699(−2)	1.90(−2)	5.2206(−2)	1.9514(−2)
$(2p4s)^1P_1^o$	6.8000(−3)	4.78(−3)	6.17384(−3)	6.61483(−3)	6.20(−3)	1.8183(−2)	6.3943(−3)
$(2p5s)^1P_1^o$	2.8927(−3)	2.22(−3)	2.79293(−3)	2.86642(−3)	2.77(−3)	8.2208(−3)	2.8297(−3)
$(2p6s)^1P_1^o$	1.5021(−3)			1.54346(−3)	1.49(−3)	4.3952(−3)	1.7272(−3)
$(2p7s)^1P_1^o$	8.8218(−4)			8.08479(−4)		2.6239(−3)	1.0657(−3)
$(2p8s)^1P_1^o$	5.6340(−4)					1.6905(−3)	5.8798(−4)
$(2p9s)^1P_1^o$	3.8228(−4)					1.1539(−3)	1.1025(−5)
$(2p10s)^1P_1^o$	2.7147(−4)					8.2318(−4)	
$(2p11s)^1P_1^o$	1.9970(−4)					6.0636(−4)	
$(2p12s)^1P_1^o$	1.5109(−4)					4.5936(−4)	
$(2p13s)^1P_1^o$	1.1704(−4)					3.5647(−4)	
$(2p14s)^1P_1^o$	9.2534(−5)					2.8297(−4)	
$(2p15s)^1P_1^o$	7.4511(−5)					2.2784(−4)	

TABLE V. Resonance widths Γ_r (in a.u.) of doubly excited states $(2pnd)^1P_1^o$ of Be. Numbers in parentheses indicate powers of 10. Reference numbers are shown in brackets.

States	MCRRPA	[5]	[35]	[37]
$(2p3d)^1P_1^o$	3.1923(−5)	1.85(−6)	1.40(−5)	3.6749(−5)
$(2p4d)^1P_1^o$	8.2726(−6)	1.10(−6)	1.02(−5)	3.6749(−5)
$(2p5d)^1P_1^o$	3.1859(−6)		7.05(−6)	3.3074(−5)
$(2p6d)^1P_1^o$	1.5607(−6)			2.5724(−5)
$(2p7d)^1P_1^o$	9.0340(−7)			7.3498(−6)
$(2p8d)^1P_1^o$	5.9906(−7)			3.6749(−6)
$(2p9d)^1P_1^o$	4.5221(−7)			
$(2p10d)^1P_1^o$	3.9161(−7)			
$(2p11d)^1P_1^o$	3.9403(−7)			
$(2p12d)^1P_1^o$	4.6258(−7)			
$(2p13d)^1P_1^o$	6.2560(−7)			
$(2p14d)^1P_1^o$	9.4116(−7)			
$(2p15d)^1P_1^o$	1.4906(−6)			

Therefore parameters ξ and η change sign through the resonance minimum and vary reciprocally to the energy departure from the resonance minimum.

Because of the above reasons, the spin polarization parameter ζ has a maximum value 1.5 at the resonance minimum and varies reciprocally to the square of the energy departure from the resonance minimum outside the immediate neighborhood of the resonance. Furthermore, it is worth noting that although the cross section in Eq. (5) is independent of the relative phase, the resonance minimum reveal the position where the relative phase goes through π rapidly.

B. *F*-type resonances

For Rydberg series $(2pns)^3P_1^o$ and $(2pnd)^3P_1^o$ coupled to the ground state $^1S_0$ through *forbidden* transitions, photoionization parameters $\{\beta, \xi, \eta, \zeta\}$ exhibit characteristics very different from those of A type and which will be classified as of F type. Resonance $(2p3s)^3P_1^o$ and $(2p3d)^3P_1^o$ are shown in the first and second columns of Fig. 7 as a demonstration. For F-type resonances, it is the triplet amplitude D_T rather than the singlet amplitude D_S which is coupled more strongly to the resonance. Therefore in the neighborhood of F-type resonances, the singlet amplitude D_S varies more or less monotonically such that resonance structures of $\{\beta, \xi, \eta, \zeta\}$ are primarily due to variations in the triplet amplitude D_T.

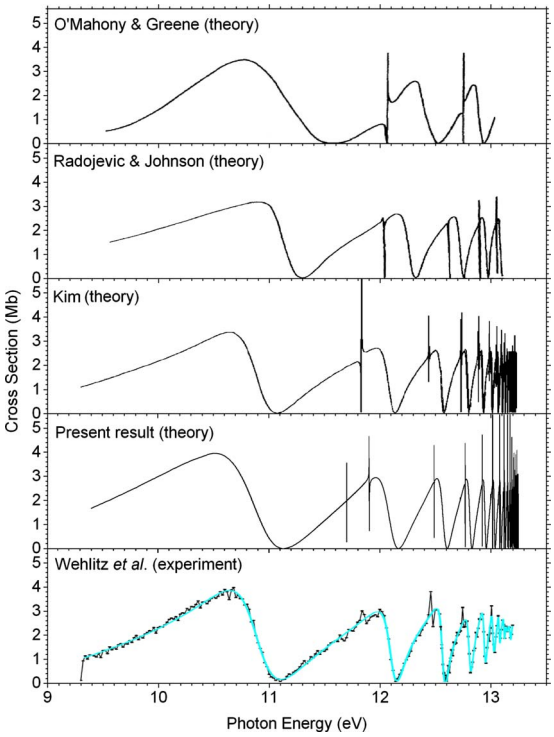

FIG. 5. (Color online) Comparison of the photoionization cross section of beryllium from the present MCRRPA calculation with those from others.

TABLE VI. Resonance energies E_r and widths Γ_r (in a.u.) of doubly excited states $(2pns)^3P_1^o$, $(2pnd)^3P_1^o$, and $(2pnd)^3D_1^o$ of Be. Numbers in brackets parentheses indicate powers of 10.

States	E_r	Γ_r	States	E_r	Γ_r	States	E_r	Γ_r
$(2p3s)^3P_1^o$	0.385166	7.5190(−4)	$(2p3d)^3P_1^o$	0.435196	5.8193(−4)	$(2p3d)^3D_1^o$	0.430064	5.5488(−8)
$(2p4s)^3P_1^o$	0.440153	2.4654(−4)	$(2p4d)^3P_1^o$	0.457713	2.7098(−4)	$(2p4d)^3D_1^o$	0.455835	3.0195(−8)
$(2p5s)^3P_1^o$	0.460260	1.1105(−4)	$(2p5d)^3P_1^o$	0.468476	1.4403(−4)	$(2p5d)^3D_1^o$	0.467582	3.8467(−8)
$(2p6s)^3P_1^o$	0.469898	5.9610(−5)	$(2p6d)^3P_1^o$	0.474406	8.4698(−5)	$(2p6d)^3D_1^o$	0.473908	5.9886(−8)
$(2p7s)^3P_1^o$	0.475266	3.5987(−5)	$(2p7d)^3P_1^o$	0.478010	5.3663(−5)	$(2p7d)^3D_1^o$	0.477701	9.3054(−8)
$(2p8s)^3P_1^o$	0.478563	2.3753(−5)	$(2p8d)^3P_1^o$	0.480359	3.5945(−5)	$(2p8d)^3D_1^o$	0.480152	1.3803(−7)
$(2p9s)^3P_1^o$	0.480733	1.6907(−5)	$(2p9d)^3P_1^o$	0.481975	2.5118(−5)	$(2p9d)^3D_1^o$	0.481827	1.9468(−7)
$(2p10s)^3P_1^o$	0.482237	1.2896(−5)	$(2p10d)^3P_1^o$	0.483133	1.8133(−5)	$(2p10d)^3D_1^o$	0.483022	2.6235(−7)
$(2p11s)^3P_1^o$	0.483322	1.0502(−5)	$(2p11d)^3P_1^o$	0.483991	1.3427(−5)	$(2p11d)^3D_1^o$	0.483905	3.3849(−7)
$(2p12s)^3P_1^o$	0.484131	9.0797(−6)	$(2p12d)^3P_1^o$	0.484645	1.0146(−5)	$(2p12d)^3D_1^o$	0.484575	4.2047(−7)
$(2p13s)^3P_1^o$	0.484749	8.2492(−6)	$(2p13d)^3P_1^o$	0.485154	7.7966(−6)	$(2p13d)^3D_1^o$	0.485095	5.0433(−7)
$(2p14s)^3P_1^o$	0.485233	7.7465(−6)	$(2p14d)^3P_1^o$	0.485559	6.0888(−6)	$(2p14d)^3D_1^o$	0.485508	5.8652(−7)
$(2p15s)^3P_1^o$	0.485619	7.3465(−6)	$(2p15d)^3P_1^o$	0.485885	4.8474(−6)	$(2p15d)^3D_1^o$	0.485840	6.6415(−7)

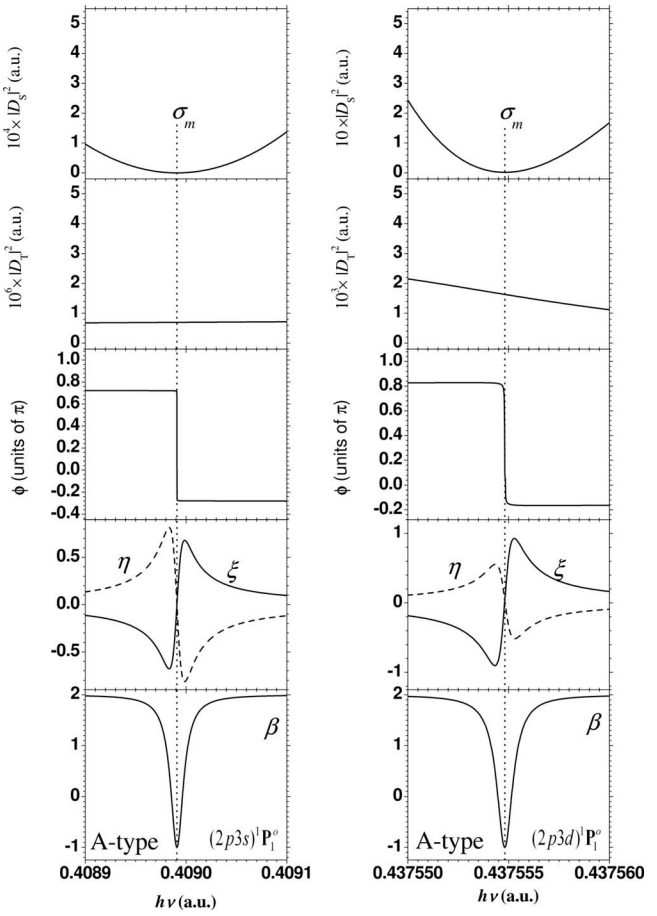

FIG. 6. Photoionization parameters $\{\beta, \xi, \eta\}$ as well as transition amplitudes $\{|D_S|^2, |D_T|^2\}$ and their relative phase ϕ for A-type resonances $(2p3s)^1P_1^o$ and $(2p3d)^1P_1^o$. Here σ_m indicates the cross-section minimum.

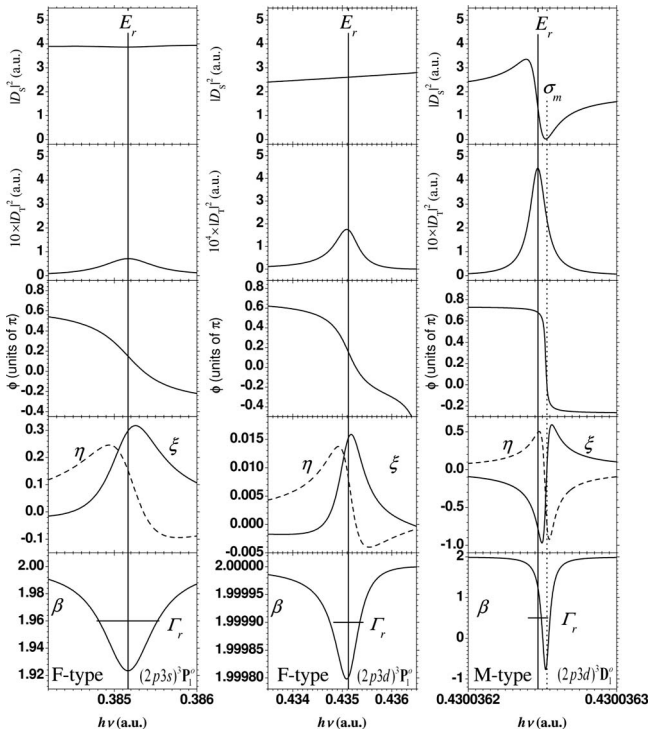

FIG. 7. Photoionization parameters $\{\beta, \xi, \eta\}$ as well as transition amplitudes $\{|D_S|^2, |D_T|^2\}$ and their relative phase ϕ for F-type resonances $(2p3s)^3P_1^o$ and $(2p3d)^3P_1^o$ and for the M-type resonance $(2p3d)^3D_1^o$. Here σ_m indicates the cross-section minimum, E_r the resonance energy, and Γ_r the width of the resonance.

The asymmetry of parameters $\{\beta, \xi, \eta, \zeta\}$ about the resonance energy E_r for resonance $(2p3s)^3P_1^o$ and $(2p3d)^3P_1^o$ depends on the slope of cross section at the resonance. Because of a small resonance structure of $|D_T|^2$ residing on a slanted large background $|D_S|^2$, the variations of parameters $\{\beta, \xi, \eta, \zeta\}$ are much smaller and less symmetric about the resonance energy E_r, compared to those of singlet resonances. It is also reasonable that the variations of β and ζ reach their extrema near the resonance energy E_r for resonance $(2p3s)^3P_1^o$, and the half-width of the variations is also approximately the resonance width Γ_r.

C. *M*-type resonances

Resonances $(2pnd)^3D_1^o$, which resemble a *mixture* of A-type and F-type resonances, are classified as of M type. Results for resonance $(2p3d)^3D_1^o$ are shown in the third column of Fig. 7. The transition amplitude D_S varies dramatically around A-type resonances, while the transition amplitude D_T varies around F-type resonances. However, because of much stronger spin-orbit couplings, resonances $(2pnd)^3D_1^o$ induce resonance structures in D_S as well as in D_T. As shown in Fig. 7, the resonance structure of $\{\beta, \xi, \eta, \zeta\}$ for the M-type resonance $(2p3d)^3D_1^o$ takes place at the resonance energy E_r, which resembles that of F type, whereas a very deep cross section minimum also occurs near the $(2p3d)^3D_1^o$ resonance structure, similar to that of A type.

IV. CONCLUSION

Resonance energies E_r and widths Γ_r of all five Rydberg series, $(2pns)^1P_1^o$, $(2pns)^3P_1^o$, $(2pnd)^1P_1^o$, $(2pnd)^3P_1^o$, and $(2pnd)^3D_1^o$, of doubly excited states between $(1s^22s)^2S_{1/2}$ and $(1s^22p)^2P_{1/2}$ ionization thresholds of beryllium atom are studied in detail including correlation and relativistic effects. The positions of resonance energies E_r are in general agreement with previous experiments and theoretical calculations. The resonance widths also agree well with those of other theories and with experiment. On the other hand, experimental data are only available for the energies E_r and widths Γ_r of two singlet Rydberg series $(2pns)^1P_1^o$ and $(2pnd)^1P_1^o$.

The angular-distribution and spin-polarization parameters $\{\beta, \xi, \eta, \zeta\}$, which have pronounced variations in the vicinity of each double-excitation resonance, display primarily three classes of characteristic behaviors: namely, A type for *allowed* resonances $(2pns)^1P_1^o$ and $(2pnd)^1P_1^o$, F type for *forbidden* resonances $(2pns)^3P_1^o$ and $(2pnd)^3P_1^o$, and M type for *forbidden* resonances $(2pnd)^3D_1^o$ with large spin-orbit coupling effects.

However, as apparent from Fig. 7, it is possible to obtain experimentally both energies and widths of the triplet Rydberg series $(2pns)^3P_1^o$, $(2pnd)^3P_1^o$, and $(2pnd)^3D_1^o$ by measuring the photoelectron angular-distribution parameter β. Nevertheless, for this purpose, spin-polarization measurements of photoelectrons could always be independent verifications. Experimental studies on angular distribution of photoelectrons are suggested to obtain information on widths of some states, which cannot be obtained from total cross-section measurements.

ACKNOWLEDGMENT

This research was supported in part by the National Science Council of the Republic of China under Grant No. NSC95-2112-M-001-053-MY3

[1] H. P. Kelly, Phys. Rev. **136**, B896 (1964).
[2] H. P. Kelly and R. L. Symon, Phys. Rev. Lett. **30**, 529 (1973).
[3] T. N. Chang, J. Phys. B **13**, L551 (1980).
[4] Z. Altun, S. L. Carter, and H. P. Kelly, Phys. Rev. A **27**, 1943 (1983).
[5] D. L. Moores, Proc. Phys. Soc. London **91**, 830 (1967).
[6] B. G. Burke and D. L. Moores, J. Phys. B **1**, 575 (1968).
[7] J. Dubau and J. Wells, J. Phys. B **6**, L31 (1973).
[8] J. Dubau and J. Wells, J. Phys. B **6**, 1452 (1973).
[9] C. Medoza and C. J. Zeippen, Astron. Astrophys. **179**, 346 (1987).
[10] P. L. Altick, Phys. Rev. **169**, 21 (1968).
[11] G. N. Bates and P. L. Altick, J. Phys. B **6**, 653 (1973).
[12] R. Moccia and P. Spizzio, J. Phys. B **18**, 3537 (1985).
[13] T. N. Chang, Phys. Rev. A **36**, 5468 (1987).
[14] R. Moccia and P. Spizzo, Phys. Rev. A **39**, 3855 (1989).
[15] C. Laughlin and G. A. Victor, in *Atomic Physics 3*, edited by S. J. Smith and G. K. Waters (Plenum, New York, 1972), p. 247.
[16] T. N. Rescigno, Phys. Rev. A **31**, 607 (1985).
[17] C. H. Greene, Phys. Rev. A **23**, 661 (1981).
[18] P. F. O'Mahony and C. H. Greene, Phys. Rev. A **31**, 250 (1985).
[19] P. L. Altick and A. E. Glassgold, Phys. Rev. **133**, A632 (1964).
[20] M. Y. Amusia, N. A. Cherepkov, D. Zivanovic, and V. Radojevic, Phys. Rev. A **13**, 1466 (1976).
[21] W. R. Johnson and C. D. Lin, J. Phys. B **10**, L331 (1977).
[22] P. C. Deshmukh and S. T. Manson, Phys. Rev. A **28**, 209 (1983).
[23] V. Radojevic and W. R. Johnson, Phys. Rev. A **31**, 2991 (1985).
[24] C. Froese Fisher and H. P. Saha, Can. J. Phys. **65**, 772 (1987).
[25] M. Aymer, J. Phys. B **20**, 6507 (1987).
[26] K.-N. Huang and W. R. Johnson, Phys. Rev. A **25**, 634 (1982).
[27] W. R. Johnson and K.-N. Huang, Phys. Rev. Lett. **48**, 315 (1982).
[28] K.-N. Huang, Phys. Rev. A **26**, 734 (1982).
[29] H.-C. Chi, K.-N. Huang, and K. T. Cheng, Phys. Rev. A **43**, 2542 (1991).
[30] G. Mehlman-Balloffet and J. M. Esteva, Astrophys. J. **157**, 945 (1969).
[31] J. M. Esteva, G. Mehlman-Balloffet, and J. Romand, J. Quant. Spectrosc. Radiat. Transf. **12**, 1291 (1972).
[32] R. Wehlitz, D. Lukic, and B. Bluett, Phys. Rev. A **68**, 052708 (2003).
[33] C. M. Lee and W. R. Johnson, Phys. Rev. A **22**, 979 (1980).
[34] C. D. Lin, J. Phys. B **16**, 723 (1983).
[35] T. N. Chang and L. Zhu, Phys. Rev. A **48**, R1725 (1993).
[36] B. Zhou and C. D. Lin, Phys. Rev. A **51**, 1286 (1995).
[37] D.-S. Kim, S. S. Tayal, H.-L. Zhou, and S. T. Manson, Phys. Rev. A **61**, 062701 (2000).
[38] K.-N. Huang, H.-C. Chi, and H.-S. Chou, Chin. J. Phys. (Taipei) **33**, 565 (1995).
[39] J. A. Tully, M. J. Seaton, and K. A. Berrington, J. Phys. B **23**, 3811 (1990).
[40] H.-S. Chou and K.-N. Huang, Chin. J. Phys. (Taipei) **35**, 35 (1997).
[41] H.-C. Chi and K.-N. Huang, Phys. Rev. A **50**, 392 (1994).
[42] C.-M. Wu, H.-C. Chi, and K.-N. Huang, J. Phys. B **27**, 3927 (1994).
[43] L.-R. Wang, H.-C. Chi, and K.-N. Huang, Phys. Rev. Lett. **83**, 702 (1999).
[44] A. A. Wills, T. W. Gorczyca, N. Berrah, B. Langer, Z. Felfli, E. Kukk, J. D. Bozek, O. Nayandin, and M. Alshehri, Phys. Rev. Lett. **80**, 5085 (1998).
[45] H.-C. Chi and K.-N. Huang, Phys. Rev. A **43**, 4742 (1991).
[46] M. D. Lindsay, L.-T. Cai, G. W. Schinn, C.-J. Dai, and T. F. Gallagher, Phys. Rev. A **45**, 231 (1992).
[47] L.-R. Wang, J.-T. Hsiao, and K.-N. Huang, J. Phys. B **39**, L217 (2006).
[48] K.-N. Huang, Am. J. Phys. **62**, 73 (1994).
[49] K.-N. Huang, Phys. Rev. A **22**, 223 (1980).
[50] K.-N. Huang, Phys. Rev. Lett. **48**, 1811 (1982).
[51] K.-N. Huang, Phys. Rev. A **26**, 3676 (1982).